IEEE Access
Multidisciplinary | Rapid Review | Open Access Journal

Received February 22, 2022, accepted March 21, 2022, date of publication March 25, 2022, date of current version March 31, 2022.

Digital Object Identifier 10.1109/ACCESS.2022.3162262

Analysis of Radome Cross Section of an Aircraft Equipped With a FSS Radome

HOKEUN SHIN[1], (Member, IEEE), DAEYEONG YOON[2], (Student Member, IEEE), DONG-YEOP NA[3], (Member, IEEE), AND YONG BAE PARK[2,4], (Senior Member, IEEE)

[1]Naval Research and Development Center Pangyo Part, Hanwha Systems, Seongnam 13524, South Korea
[2]Department of AI Convergence Network, Ajou University, Suwon 16499, South Korea
[3]School of Electrical and Computer Engineering, Purdue University, West Lafayette, IN 47907, USA
[4]Department of Electrical and Computer Engineering, Ajou University, Suwon 16499, South Korea

Corresponding author: Yong Bae Park (yong@ajou.ac.kr)

This work was supported in part by the Basic Science Research Program through the National Research Foundation of Korea (NRF) funded by the Ministry of Science and ICT (MSIT) under Grant 2020R1A2B5B01002251; and in part by the NRF Grant funded by the Korea Government, MSIT, under Grant 2021R1A4A1030775.

ABSTRACT We study the radar cross section (RCS) property of an aircraft considering the electromagnetic (EM) characteristics of a frequency selective surface (FSS) radome, mounted on the aircraft. Instead of full-wave methods, we utilize high-frequency methods, such as the shooting and bouncing rays (SBR), physical theory of diffraction (PTD), and flat model, taking a significant computational efficiency. Based on the developed algorithm, we analyze monostatic and bistatic RCSs of the aircraft equipped with either single- and multi-layer dielectric, FSS, or PEC radomes in terms of frequency and polarization. Our calculations are validated by comparing with those of the commercial EM simulator with significant computational efficiency. The present numerical study indicates that including the radome EM characteristics into the overall aircraft RCS study is crucial for the accurate RCS estimate

INDEX TERMS Frequency selective surface (FSS), FSS radome, radar cross section (RCS), shooting and bouncing rays (SBR), physical theory of diffraction (PTD), flat model.

I. INTRODUCTION

Rapid technological advances in radar systems have made it possible to detect the appearance of enemy aircraft early with a higher probability in real time. Conversely, the viability of friendly aircraft is increasingly threatened [1]. Therefore, modern aircraft designs require a much smaller radar cross-section (RCS), which indicates how well radar can detect an object to better evade radar detection [3]–[5].

Current electromagnetic (EM) stealth technology is primarily focused on developing these RCS reduction capabilities. During this stealth-oriented design, it is important to evaluate and predict the RCS characteristics of the designed aircraft. [1], [2]. Analytical formulations are often limited to calculating scattered EM fields in objects of arbitrary geometric complexity, and there must be an accurate, reliable and fast computational electromagnetic (CEM) algorithm for RCS estimation. Some previous studies have evaluated the RCS of aircraft using the full-wave method such as finite differential time domain (FDTD) [6], method of moments (MoM) [7]–[10] and multi-level fast multi-pole method (MLFMM) [11]–[15]. Full-wave EM analysis can yield very accurate results, but it is computationally expensive and may present some minor issues when dealing with electrically large structures. In particular, differential equation solvers such as FDTD and finite element methods (FEM) must implement costly volumetric discretization for both absorption boundary conditions (e.g. perfectly matched layers) and scatterers and surrounding space. In addition, integral equation solvers requires the costly inversion of full matrices and preconditioners to treat the ill-conditioning issue. Alternatively, high-frequency technology based on the shooting and bouncing rays (SBR) can be utilized to evaluate an aircraft's RCS much more efficiently. Several previous studies successfully showed the aircraft RCS study using the high-frequency methods [15]–[22]. The SBR method was used to analyze the RCS of various aircrafts including scale down models [15]–[17] and full-scale models [16]–[19], which were assumed as a perfect electric conductor (PEC). In addition, the RCS of aircrafts full- [20] and partially

The associate editor coordinating the review of this manuscript and approving it for publication was Davide Comite.

coated [21], [22] with radar absorbing materials (RAM) was evaluated using the SBR method.

However, most previous work on the RCS of aircraft assumed a fuselage-mounted radome as a PEC. These naive assumptions fail to capture the effects of modern radomes on an aircraft's overall RCS performance, which can lead to significant deviations between numerical calculations and measured data. For example, recent studies have shown that the use of multi-layered dielectric or frequency selective surface (FSS) radomes could achieve the considerable reduction of the RCS, caused by the antenna mounted on the front of the fuselage [23]–[29], instead of using a single-layered dielectric radome. This indicates that explicit consideration of the EM characteristics of the radome is essential for an accurate evaluation of the aircraft RCS properties. A recent study performed RCS analysis of a hemispherical FSS radome mounted on a simple circular cylinder [28], [29], but RCS studies of aircraft with complex radome structures have not yet been performed.

In this paper, the RCS of an aircraft equipped with a tangential FSS radome, which is a curved hash-shaped slot FSS unit cell built into a multi-layered radome, was analyzed. Using a hybrid approach using both full-wave and high-frequency methods, we utilize the flat model and SBR method [27], [30] to describe the scattered EM fields inside the aircraft based on ray physics. Furthermore, we consider diffraction fields generated at edges of the aircraft via physical theory of diffraction (PTD) [1] to improve the accuracy of the present method. Meanwhile, the transmission and reflection behaviors of the inserted FSS layer at given incident angles for parallel and perpendicular polarization are extracted using a commercial full-wave EM solver (ANSYS HFSS [31]). It is then incorporated into the planar model for subsequent use of the high-frequency method.

The first two calculations are the monostatic RCS of a single-layer dielectric radome mounted on a PEC disk and a multi-layer dielectric radome mounted on a missile. The results are compared with those of a commercial EM solver (Microwave Studio (MWS) of CST) [32] for validation. Then, calculate the bistatic RCS of aircraft equipped with FSS, dielectric, or PEC radomes to understand stealth performance. Numerical results show that the inclusion of the EM characteristics of FSS radomes in aircraft RCS studies results in significant deviations (up to approximately 40 dBsm difference) from PEC radomes.

II. ANALYSIS PROCEDURE

A. MODELING OF THE AIRCRAFT EQUIPPED WITH THE FSS RADOME

Fig. 1 depicts the problem geometry illustrating an aircraft equipped with a FSS radome. The aircraft is a simplified model of a stealth fighter whose fuselage is assumed to be a PEC. The length and wingspan of the aircraft are 18.97 m and 13.65 m, respectively. The antenna enclosed by the FSS radome is in the surface of the front of the fuselage. Here, we consider the same tangent-ogive FSS radome used in [27],

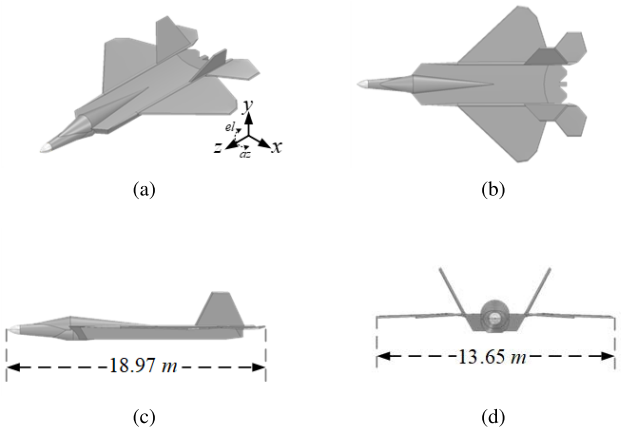

FIGURE 1. Problem geometry of an aircraft under this study. (a) Full three-dimensional, (b) xz plane, (c) yz plane, and (d) xy plane views.

which has a passband characteristic in the X-band. The base diameter and height of the FSS radome are 800 mm and 1060 mm, respectively. The FSS radome consist of seven layers: the innermost and outermost layers are E-glass/epoxy (skin), second and sixth layers are foam, third and fourth layers are adhesive films, and a FSS layer (hash- shaped slot unit cells) is sandwiched by the adhesive films. A detailed configuration and dimension of the FSS radome can be found in [27].

B. NUMERICAL METHOD FOR RCS ESTIMATE

The problem geometry under this study consists of a PEC fuselage equipped with the multi-layer radome, which embeds a curved FSS layer. To calculate the RCS of the aircraft, we use the SBR method, PTD, and the flat model. The SBR method and PTD are well-known high-frequency techniques that can efficiently analyze the RCS of electrically large objects such as naval ships and aircrafts [33], [34]. The SBR method is based on the ray tracing technique and physical optics (PO), which can quantify the multiple reflections by determining the equivalent current densities induced on the surface of illuminated PEC planes, whereas PTD can calculate the diffraction fields based on the determination of the filamentary currents induced on illuminated of PEC edges. In addition, the ray tracing technique and flat model are useful for identifying the EM characteristics of a multi-layer radome [27], [30]. In the high-frequency regime, the curved radome can be looked locally flat via the tangent plane approximation where the phase matching condition fulfills locally. Note that ''flat model'' refers to a flat multi-layer radome with the same structure as an original curved radome. This method uses a look-up table including the pre-computed reflection and transmission coefficients of the flat model, which can significantly reduce the costly computational loads. Therefore, the present method is highly suitable for the EM analysis of a multi-layer radome embedding a curved FSS layer. Fig. 2 shows the analysis procedure to calculate the RCS of the aircraft equipped with the FSS radome based on the SBR method, PTD, and flat model.

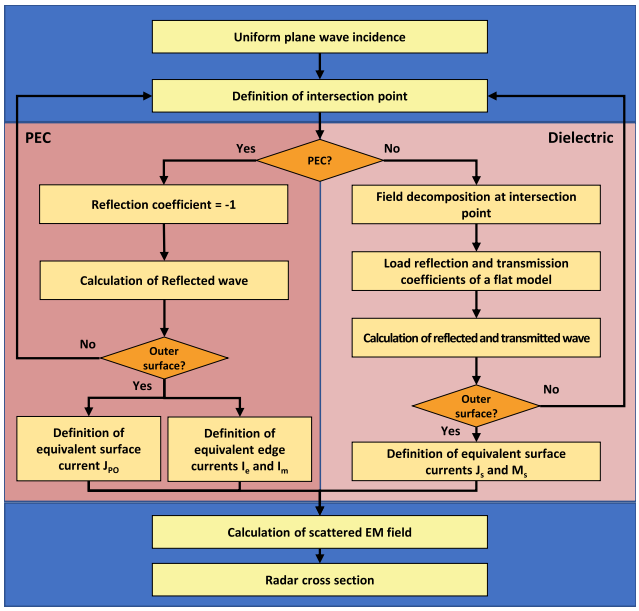

FIGURE 2. Algorithmic flow of the present method for calculating the RCS of an aircraft mounted on the FSS radome.

1) RAY TRACING WITH FLAT MODEL

An incident plane wave illuminating the aircraft is modeled by numerous rays. Then, the intersection points where the rays hit the aircraft are determined, and the perpendicular($\vec{e}_\perp$) and parallel vector ($\vec{e}_\parallel$) are calculated by using the ray direction vector($\vec{k} = (k_x, k_y, k_z)$) and the radome surface normal vector($\hat{n} = (n_x, n_y, n_z)$) in eqs. (1).

$$\begin{aligned} \vec{e}_\perp &= \hat{n} \times \vec{k} \\ \vec{e}_\parallel &= \vec{e}_\perp \times \vec{k} \end{aligned} \tag{1}$$

The electric field can be decomposed by using normalized perpendicular($\hat{e}_\perp$) and parallel vector($\hat{e}_\parallel$) in eqs. (2).

$$\begin{aligned} \vec{E}_\perp &= \vec{E} \times \vec{e}_\perp \\ \vec{E}_\parallel &= \vec{E} \times \vec{e}_\parallel \end{aligned} \tag{2}$$

If the intersection point is placed on PEC surfaces, such as the metal tip, the enclosed antenna, and the fuselage, there are only reflected waves phase reversed in eqs. Otherwise, the reflected and transmitted waves are calculated using reflection(Γ) and transmission(T) coefficients pre-computed from the flat model. We determined the reflection($\vec{E}_r$) and transmission electric field($\vec{E}_t$) at intersection point in eqs. (3).

$$\begin{aligned} \vec{E}_r &= \Gamma_\perp \vec{E}_\perp + \Gamma_\parallel \vec{E}_\parallel \\ \vec{E}_t &= T_\perp \vec{E}_\perp + T_\parallel \vec{E}_\parallel \end{aligned} \tag{3}$$

For example, when a transmitted wave pass through the FSS, it is reflected by the enclosed antenna and then the reflected wave is traced until it reaches the outermost surface (see Fig. 3).

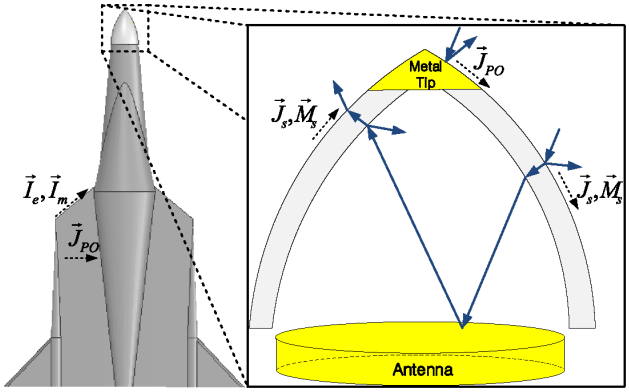

FIGURE 3. Illustration of the analysis procedure about the FSS radome structure mounted on the aircraft.

2) PHYSICAL OPTICS

Using ray tracing technology, electric($\vec{E}_a$) and magnetic fields($\vec{H}_a$) were obtained at the intersection point of the outer radome and the PEC body. The induced equivalent electric($\vec{J}_s$) and magnetic surface current ($\vec{M}_s$) on the outer radome given by

$$\begin{aligned} \vec{J}_s &= \hat{n} \times \vec{H}_a \\ \vec{M}_s &= -\hat{n} \times \vec{E}_a \end{aligned} \tag{4}$$

Similarly, for a PEC body with a reflection coefficient of -1, the induced equivalent electric($\vec{J}_{PO}$) and magnetic surface current ($\vec{M}_{PO}$) in the PEC body are given by

$$\begin{aligned} \vec{J}_{PO} &= 2\hat{n} \times \vec{H}_a \\ \vec{M}_{PO} &= 0 \end{aligned} \tag{5}$$

In the far-field condition that the distance between the source and a target is so far enough, the scattering Electric field can be approximated as

$$\vec{E}_s \approx \frac{j\beta}{4\pi r} \int_s \hat{r} \times \vec{M} - (\hat{r} \times \eta \vec{J} \times \hat{r}) e^{j\beta \hat{r} \cdot \vec{r}'} \partial s' \tag{6}$$

where r is the distance from scattering point to observation point, $\vec{r}'$ is the observation position vector, β is wavenumber, S is the surface of the facet and $\hat{r}$ is the unit position vector in S (See Fig. 4).

3) PHYSICAL THEORY OF DIFFRACTION

The PTD technique was applied to consider the diffraction at the point where the PEC edge and the ray intersect point. The filament electric (I_e) and magnetic current (I_m) were defined as in [1] and the diffracted waves were calculated as follows.

$$\vec{E}_d \approx \frac{jk}{4\pi r} \int_c (\eta I_e \hat{k}_d \times (\hat{k}_d \times \hat{z}_l) + I_m \hat{k}_d \times \hat{z}_l) e^{-j\beta \hat{r} \cdot \hat{r}'} dl' \tag{7}$$

where $\vec{r}'$ is the position of a point on C, $\hat{k}_d$ is the unit vector in the direction of diffraction and $\hat{z}_l$ is the tangent unit vector to the edge. Fig. 5. show a locally tangent wedge for diffracted field configurations.

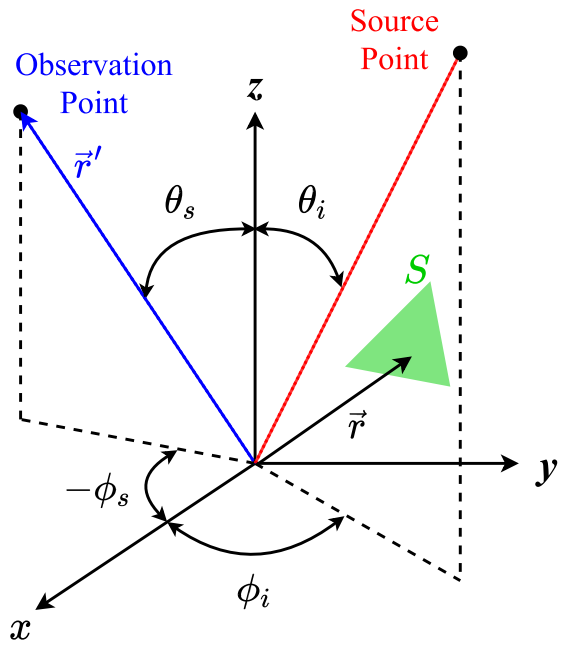

FIGURE 4. Configuration of Physical Optics for calculation of bistatic RCS. For monostatic, the observation point and the source point are the same.

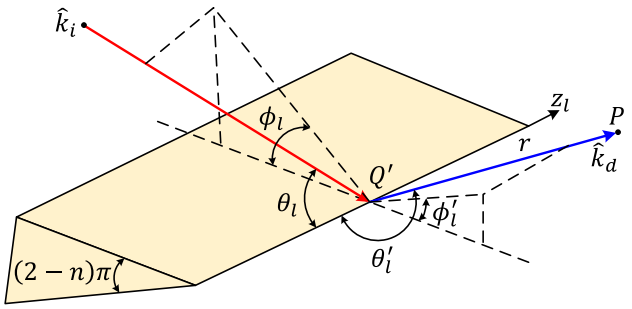

FIGURE 5. Local coordinate for compute diffraction fields.

4) RCS ESTIMATE

The total scattered electromagnetic field can be calculated as the sum of the previously calculated PO scattered field($\vec{E}_s$) and PTD scattered field($\vec{E}_d$). In [35], we can calculate RCS(σ) as the ratio of the total scattered electric field to the incident electric field at a given observation point as

$$\sigma = \lim_{r\to\infty} 4\pi r^2 \frac{|\vec{E}_s + \vec{E}_d|^2}{|\vec{E}_i|^2} \tag{8}$$

C. VALIDATE AND NUMERICAL RESULTS

Table 1 shows three models matching the X-band for RCS analysis. The single dielectric layer consists of one skin layer with half wavelength thickness. The multi dielectric layer and FSS flat model was designed previous works [31]. The multi-layer implements the 3rd and 5th layer of FSS flat model are combined into one adhesive film.

In order to analyze the EM reflection and transmission behaviors of these models, we extract the reflection and transmission coefficients at a given incident angle and frequency for both polarizations using the ANSYS HFSS [31], and configure the look-up table. Fig. 6 shows the transmission

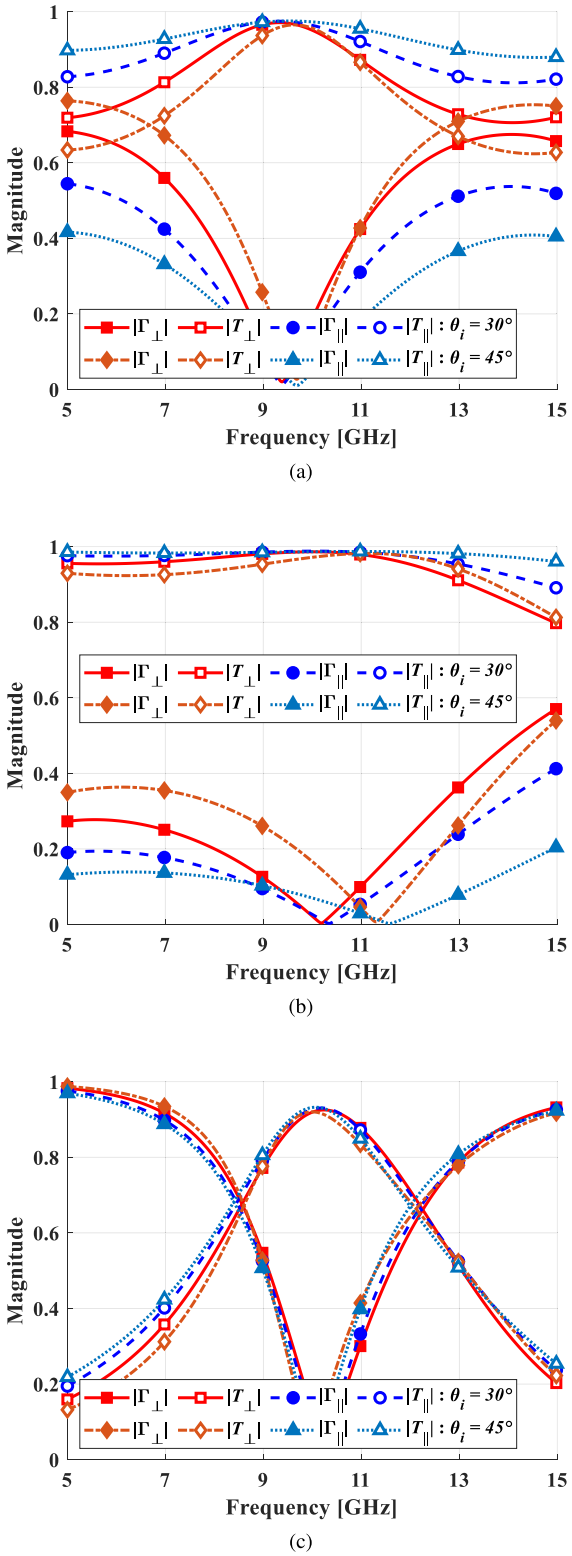

FIGURE 6. Reflection and transmission characteristic of the (a) Single-layer dielectric flat model, (b) multi-layer dielectric flat model, (c) FSS flat Model.

TABLE 1. Configuration of FSS, single, multi-layer flat model.

Flat Model	Material	ϵ_r	$\tan\delta$	Thickness	Layers
Single-layer	Skin	4.348	0.013	7.19	Single Layer
Multi-layer (5 layers)	Skin	4.348	0.013	0.84	1st, 5th
	Foam	1.103	0.0038	3.00	2nd, 4th
	Adhesive Film	3.003	0.019	0.26	3rd
FSS (7 layers)	Skin	4.348	0.013	0.84	1st, 7th
	Foam	1.103	0.0038	3.00	2nd, 6th
	Adhesive Film	3.003	0.019	0.12	3rd, 5th
	FSS (Copper)	-	-	0.02	4th

TABLE 2. Simulation conditions for RCS analysis.

Target Model	Analyze Type	Radome Material	Frequency [GHz]	Incidence θ_i, ϕ_i [°]	Observation θ_s, ϕ_s [°]
Radome	Monostatic RCS	Single	5 ~ 15	$\theta_i = 0$ $\phi_i = 0$	$\theta_s = \theta_i$ $\phi_s = \phi_i$
Missile	Monostatic RCS	Multi	10	$\theta_i \in [0,180]$ $\phi_i = 0$	$\theta_s = \theta_i$ $\phi_s = \phi_i$
	Bistatic RCS	Multi	10	$\theta_i = 0$ $\phi_i = 0$	$\theta_s \in [0,360]$ $\phi_s = 0$
Aircraft	Monostatic RCS	FSS, Multi, PEC	5 ~ 15	$\theta_i = 0$ $\phi_i = 0$	$\theta_s = \theta_i$ $\phi_s = \phi_i$
	Bistatic RCS	FSS	5, 10, 15	$\theta_i = 0$ $\phi_i = 0$	$\theta_s \in [0,360]$ $\phi_s = 0$

characteristics of the flat model versus frequencies. We confirmed that all models matched with free space about 10 GHz. Moreover, in the case of the FSS flat model in Fig. 6 (c), it shows that band-pass characteristic was distinct compared to other models.

As shown in Table 2, we calculated the RCS of 5 cases to analyze the effect of the radome and validate our numerical methods. Radome and Missile models were constructed with single and multi dielectric layers, and our method was validated by comparing simulation time, number of meshes, and root mean square error (RMSE) with commercial EM software results. RMSE is defined as

$$\text{RMSE [dB]} = \sqrt{\frac{1}{N}\sum_{n=1}^{N} |\sigma_{our} - \sigma_{cst}|^2} \tag{9}$$

where σ_{our} [dBsm] is the RCS result by the our method, and σ_{cst} [dBsm] is the RCS output by CST I-solver. RCS is computed with N sampling points in terms of frequency and angle range. Next, the RCS reduction effect of the FSS radome was analyzed by calculating the RCS of the aircraft equipped with various radomes.

For the single-layer dielectric radome mounted on a PEC disk firstly, our calculations are compared with MWS of CST

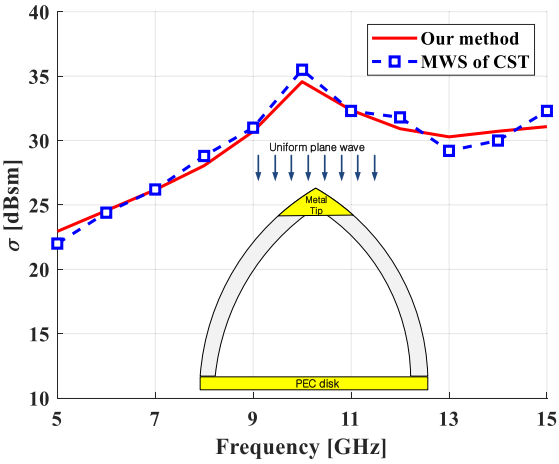

FIGURE 7. Monostatic RCS of the single-layer dielectric radome mounted on the PEC disk at $\theta_i = 0°$ and $\phi_i = 0°$ for (a) HH polarization, (b) VV polarization.

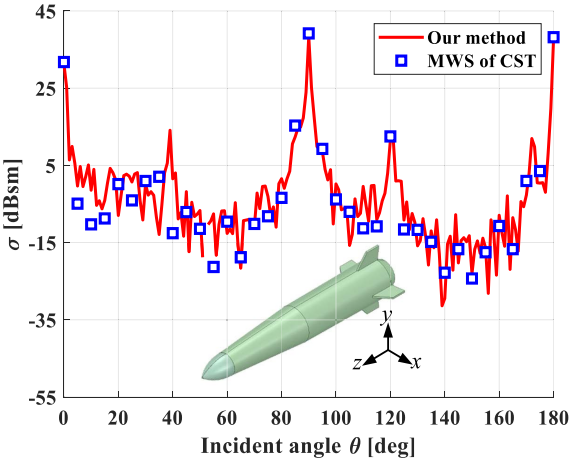

FIGURE 8. Monostatic RCS of the multi-layer dielectric radome mounted on the missile at $\phi_i = 0°$ for HH polarization.

I-solver [32] results. The PEC disk has a radius of 390 mm and is surrounded by a tangent-ogive radome with a radious

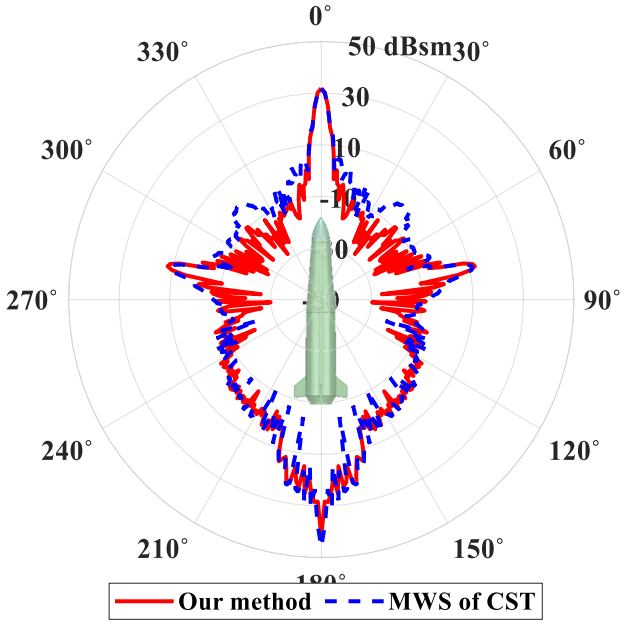

FIGURE 9. Bistatic RCS of the multi-layer dielectric radome mounted on the missile at $\theta_i = 0°$ and $\phi_i = 0°$ for HH polarization.

TABLE 3. Summary of comparing results between our method and MWS of CST.

Target Model	Analyze Type	Simulation Time	Number of Meshes	RMSE [dB]
Radome	Monostatic RCS	Our Method: 181 s CST: 32.6 h * At 10 GHz	Our Method: 137,103 CST: 1,181,282* * At 10 GHz	1.622 (HH) 1.690 (VV)
Missile	Monostatic RCS	Our Method: 193 s CST: 55.1 h* * Average time per each point	Our Method: 151,695 CST: 5,016,279	6.039
	Bistatic RCS	Our Method: 123 s CST: 79.1 h * Total Calculation Time at Normal Incidence	Our Method: 151,695 CST: 5,016,279	7.853

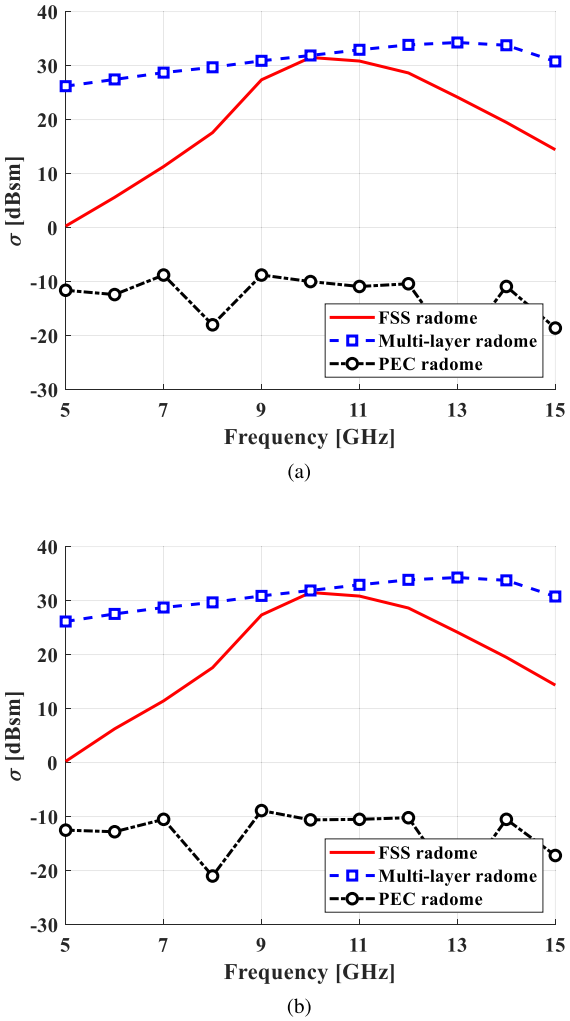

FIGURE 10. Monostatic RCS of the aircraft equipped with the FSS radome at $\theta_i = 0°$ and $\phi_i = 0°$ for (a) HH polarization, (b) VV polarization.

of 400 mm and a height of 1058 mm. Fig. 7 shows the monostatic RCS calculations via our method and MWS of CST at $\theta_i = 0°$ and $\phi_i = 0°$ for horizontal and vertical polarizations in the frequency range of 5 to 15 GHz. The RMSE of monostatic RCS between CST and our method are 1.662 and 1.690 dB within the frequency range, which is an good agreement in both calculation. The computation time at 10 GHz in our method took about 181 seconds using a PC (dual Intel Xeon CPU E5-2640v4 at 2.40 GHz and DDR4 512 GB memory), whereas CST took more than a day to simulate the same. Our method has a total number of meshes of 137,103 and CST 1,181,282 (10 GHz) respectively. In our method, the mesh is determined according to the shape of geometry regardless of frequency, whereas the I-solver of CST increases the number of mesh surfaces in proportion to the electrical size, which takes a long time to calculate. Therefore, these results clearly show that our proposed method is a time-efficient method for analyzing electrical large objects.

It also analyzes and verifies multi-layer dielectric radomes mounted on missiles measuring 2.34 m and 8.05 m in width and length, respectively. The monostatic RCS simulation was performed under a frequency of 10 GHz with angles of incidence θ_i is 0 to 180° and ϕ_i is 0°. The bistatic RCS was also simulated at a frequency of 10 GHz with observation angles θ_s ranging from 0 to 360°. The results shown in Fig. 8 and 9, respectively. The surface mesh of the missile is divided into 151,695 surfaces when analyzed using our method, whereas the CST is divided into 5,5016,279 surfaces. The monostatic and bistatic RCS computation time took about 193 s and 123 s for our method and 55.1 hours and 79.1 hours for CST. The RMSE with our method with CST shows an approximate good fit of 6.039 dB for monostatic and 7.853 dB for bistatic RCS. Table 3 summarizes the comparison between the proposed technique and CST results.

Now consider an FSS radome mounted on an aircraft (see Figure 1 for the problem geometry). Utilize the flat model results to compute the fixed RCS versus frequency of an FSS radome equipped aircraft at $\theta_i = 0°$ and $\phi_i = 0°$,

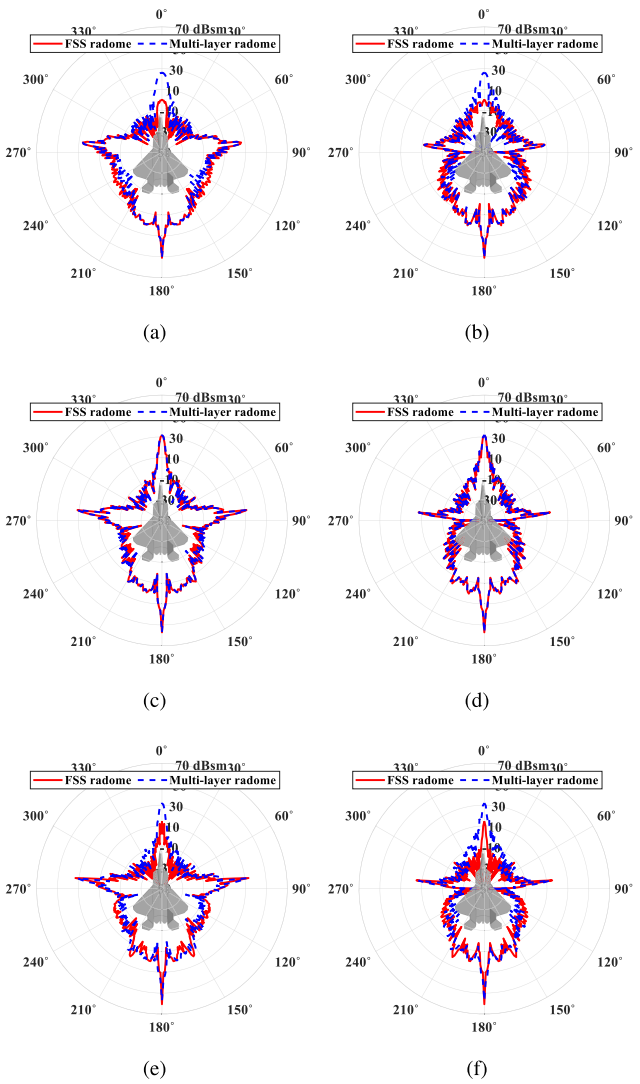

FIGURE 11. Co-polarization bistatic RCS of the aircraft equipped with the FSS radome at $\theta_i = 0°$ and $\phi_i = 0°$ for (a) HH polarization at 5 GHz, (b) VV polarization at 5 GHz (c) HH polarization at 10 GHz, (d) VV polarization at 10 GHz (e) HH polarization at 15 GHz, (f) VV polarization at 15 GHz.

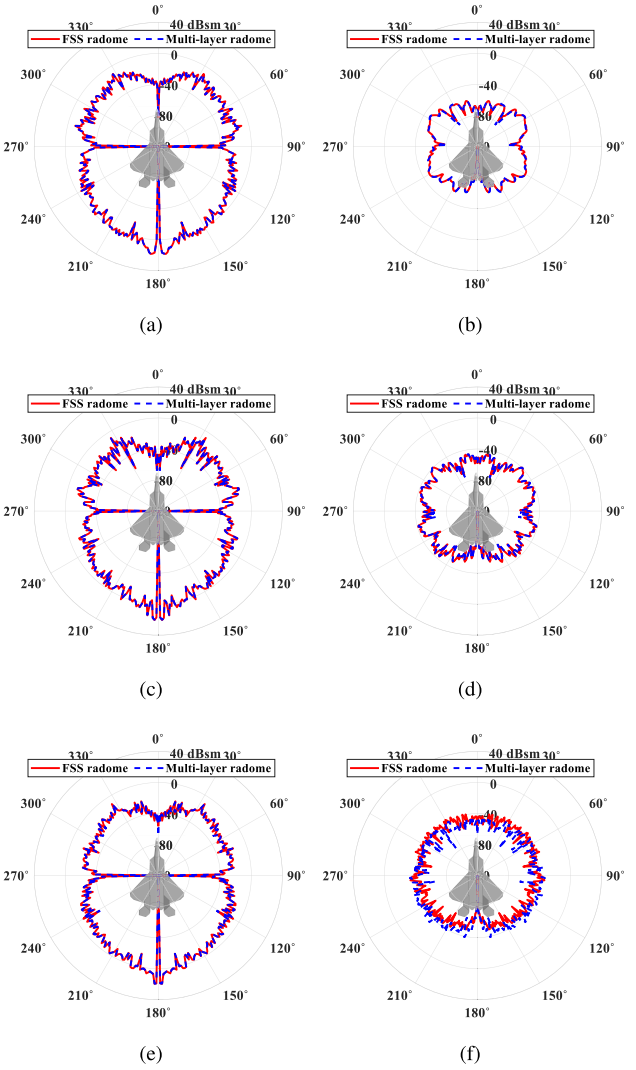

FIGURE 12. Cross-polarization bistatic RCS of the aircraft equipped with the FSS radome at $\theta_i = 0°$ and $\phi_i = 0°$ for (a) HV polarization at 5 GHz, (b) VH polarization at 5 GHz (c) HV polarization at 10 GHz, (d) VH polarization at 10 GHz (e) HV polarization at 15 GHz, (f) VH polarization at 15 GHz.

as shown in Fig. 10. It also calculates the monostatic RCS of multi-layer dielectric radome and PEC radome and compares the performance of three different radomes mounted on the aircraft. Due to the broadband transmission characteristics and high reflection from the enclosed antenna, the multi-layer dielectric radome shows a higher RCS over the entire bandwidth. On the other hand, the RCS of the FSS radome is much lower than that of the dielectric radome except for the X-band due to its passband characteristic. However, PEC radome shows completely different results because the original EM properties of the radome and enclosed antenna are not considered. The results including the EM characteristics of the FSS radome into the aircraft RCS have a significant deviation from that of the PEC radome, which is about 40 dBsm difference at most. In addition, when θ_i is 0° and ϕ_i is 0° consider the aircraft's bistatic RCS in the stopband and passband. Fig. 11 shows the bistatic RCS of the aircraft equipped with the FSS radome at 5, 10, and 15 GHz, respectively. In the bistatic RCS results at 5GHz and 15GHz (see Fig. 11 (a), (b), (e) and (f)), compared to the multi-layer dielectric radome, the FSS radome remarkably decreases the RCS (about 25.6 dBsm at most) in front of the aircraft, while it slightly increases the RCS (about 8.4 dBsm at most) around the observation angles of about 120 and 240. This is because the incident wave is mostly reflected on the surface of the FSS radome due to its stopband characteristic. On the other hand, since the incident wave is hardly reflected on the surface of the FSS radome due to its passband characteristic at 10GHz, and is mostly through the FSS radome and is reflected by the enclosed antenna, the RCS of the aircraft equipped with the FSS radome is very similar with that of the aircraft equipped with the multi-layer dielectric radome (see Fig. 11 (c), (d)). In contrast, in the cross polarization bistatic RCS, it can be seen in Fig. 12 that the significant difference due to the FSS radome is small.

TABLE 4. Comparison table of studies related to aircraft RCS estimation.

Studies	Analyze Model	Material	Analyze Method	Frequency
[5]	Real Aircraft	Mooney 231	Measurement	X band
[6]	Small Wire-grid Aircraft	PEC	FDTD	HF band
[9]	Aircraft	PEC with Thin Dielectric sheet	CBFM based on MLFMM	VHF band
[10]	Aircraft	PEC with RAM	LCM based on HOMOM	1 GHz
[15]	Aircraft	PEC	SBR, MLFMM	0.5, 1.0, 1.5, 2.0 GHz
Out Method	Aircraft mounted on FSS Radome	PEC with FSS	Flat model based on SBR	5, 10, 15 GHz

* CBFM: Characteristic Basis Function Method, LCM: Locally Coating Method

It was confirmed that the FSS radome can effectively reduce the RCS in front of the aircraft in a wide frequency range due to its passband or stopband characteristics. Moreover, in order to accurately calculate the RCS of the radome mounted on the fuselage, the EM characteristics of the radome have to be considered. Table 3 summarizes the studies and methods used for the analysis of the Aircraft model. Our method can efficiently calculate the RCS of an aircraft equipped with an FSS radome. The technique we propose can be useful for stealth design.

III. CONCLUSION

In this paper, the RCS of tangent-ogive FSS radome mounted on a fighter is calculated. Multiple reflections inside the radome were considered using the SBR technique. In addition, the reflected and transmitted EM fields were calculated using a flat model. The scattered EM field was calculated by applying the PO and PTD to the outermost part of the radome, the surface of the conductor, and the edge of the conductor, respectively. The proposed method was verified using CST, a commercial analysis program, and is very efficient in terms of the required number of meshes and calculation speed.

The RCS of the FSS radome mounted on the fuselage was smaller than that of the dielectric radome mounted on the fuselage. FSS radome can reduce the RCS of aircraft over a wide frequency range except for the pass band due to its pass band characteristic. Importantly, the RCS results will be erroneous if the EM properties of the radome are not properly taken into account. Therefore, to obtain accurate RCS results of the aircraft, the EM characteristics of the fuselage-mounted radome must be considered. The proposed method is useful for analyzing the RCS of the FSS radome mounted on fuselages such as aircrafts and missiles, and these results can be used for the stealth design.

ACKNOWLEDGMENT

(Hokeun Shin and Daeyeong Yoon are co-first authors.)

REFERENCES

[1] E. F. Knott, J. F. Schaeffer, and M. T. Tuley, *Radar Cross Section*, 2nd ed. Edison, NJ, USA: SciTech Publishing, 2004.

[2] D. J. Kozakoff, *Analysis of Radome-Enclosed Antennas*, 2nd ed. Norwood, MA, USA: Artech House, 2010.

[3] C. Bares, C. Brousseau, and A. Bourdillon, "A multifrequency HF-VHF radar system for aircraft identification," in *Proc. IEEE Int. Radar Conf.*, Arlington, VA, USA, May 2005, pp. 478–482.

[4] Y. S. Shesnokov and M. V. Krutikov, "Bistatic RCS of aircrafts at the forward scattering," in *Proc. Int. Radar Conf.*, Beijing, China, 1996, pp. 156–159.

[5] A. Jain and I. Patel, "Dynamic imaging and RCS measurements of aircraft," *IEEE Trans. Aerosp. Electron. Syst.*, vol. 31, no. 1, pp. 211–226, Jan. 1995.

[6] C. W. Trueman, S. J. Kubina, S. R. Mishra, and C. L. Larose, "RCS of small aircraft at HF frequencies," in *Proc. Symp. Antenna Technol. Appl. Electromagn. (ANTEM)*, Ottawa, ON, Canada, 1994, pp. 151–157.

[7] A. David, C. Brousseau, and A. Bourdillon, "Simulations and measurements of a radar cross section of a Boeing 747–200 in the 20–60 MHz frequency band," *Radio Sci.*, vol. 38, no. 4, pp. 1–3, 2003.

[8] G. Zhenghong and W. Mingliang, "An efficient algorithm for calculating aircraft RCS based on the geometrical characteristics," *Chin. J. Aeronaut.*, vol. 21, no. 4, pp. 296–303, 2008.

[9] Y.-R. Jeong, C.-S. Park, Y.-K. Ko, and J.-G. Yook, "Analysis of RCS of low observable aircraft in VHF band," *Int. J. Antennas Propag.*, vol. 2018, Apr. 2018, Art. no. 5435837.

[10] H. Zeng, X. Zhao, Q. Su, Y. Zhang, and H. Li, "Fast coating analysis and modeling for RCS reduction of aircraft," *Chin. J. Aeronaut.*, vol. 32, no. 6, pp. 1481–1487, 2019.

[11] J. C. Bowman, "Methods for rapid computation of RCS in aircraft design," in *Proc. IEEE Nat. Aerosp. Electron. Conf. (NAECON)*, Dayton, OH, USA, Oct. 2005, pp. 118–125.

[12] X. Fan, Y. Qin, S. Shang, D. Song, W. Sun, D. Li, and X. Luo, "Research on the bastatic RCS characteristics of stealth aircraft," in *Proc. Asia–Pacific Microw. Conf. (APMC)*, Nanjing, China, 2015, pp. 1–3.

[13] L. Gürel, H. Bağcı, J. C. Castelli, A. Cheraly, and F. Tardivel, "Validation through comparison: Measurement and calculation of the bistatic radar cross section of a stealth target," *Radio Sci.*, vol. 38, no. 3, pp. 1–12, 2003.

[14] L. Zhanhe, H. Peilin, G. Xu, L. Ying, and J. Zu, "Multi-frequency RCS reduction characteristics of shape stealth with MLFMA with improved MMN," *Chin. J. Aeronaut.*, vol. 23, no. 3, pp. 327–333, Jun. 2010.

[15] A. Bilal, S. M. Hamza, Z. Taj, and S. Salamat, "Comparison of SBR and MLFMM techniques for the computation of RCS of a fighter aircraft," *IET Radar, Sonar Navigat.*, vol. 13, no. 10, pp. 1805–1810, Oct. 2019.

[16] K. Yue, Y. Gao, G. Li, and D. Yu, "Conceptual design and RCS performance research of shipborne early warning aircraft," *J. Syst. Eng. Electron.*, vol. 25, no. 6, pp. 968–976, Dec. 2014.

[17] K. Yue, W. Liu, G. Li, J. Ji, and D. Yu, "Numerical simulation of RCS for carrier electronic warfare airplanes," *Chin. J. Aeronaut.*, vol. 28, no. 2, pp. 545–555, Feb. 2015.

[18] L. Zhu, X. Liang, J. Li, and R. Li, "Simulation analysis on static scattering characteristics of stealth aircraft," in *Proc. IEEE Adv. Inf. Manage., Commun., Electron. Autom. Control Conf. (IMCEC)*, Xi'an, China, Oct. 2016, pp. 3–5.

[19] T.-T. Feng and L.-X. Guo, "An improved ray-tracing algorithm for SBR-based EM scattering computation of electrically large targets," *IEEE Antennas Wireless Propag. Lett.*, vol. 20, no. 5, pp. 818–822, May 2021.

[20] M. A. Alves, R. J. Port, and M. C. Rezende, "Simulation of the radar cross section of a stealth aircraft," in *Proc. SBMO/IEEE MTT-S Int. Microw. Optoelectron. Conf.*, Salvador, Brazil, Oct./Nov. 2007, pp. 409–412.

[21] L. A. de Andrade, L. S. C. dos Santos, and A. M. Gama, "Analysis of radar cross section reduction of fighter aircraft by means of computer simulation," *J. Aerosp. Technol. Manage.*, vol. 6, no. 2, pp. 177–182, 2014.

[22] R. Brem and T. F. Eibert, "A shooting and bouncing ray (SBR) modeling framework involving dielectrics and perfect conductors," *IEEE Trans. Antennas Propag.*, vol. 63, no. 8, pp. 3599–3609, Aug. 2015.

[23] W. Tian, X. Hou, and Y. Che, "The analysis and measurement of FSS radome for antenna RCS reduction," in *Proc. Cross Tsrait Quad-Regional Radio Sci. Wireless Technol. Conf.*, Chengdu, China, 2013, pp. 297–299.

[24] J. H. Kim, H. J. Chun, I. P. Hong, Y. J. Kim, and Y. B. Park, "Analysis of FSS radomes based on physical optics method and ray tracing technique," *IEEE Antennas Wireless Propag. Lett.*, vol. 13, pp. 868–871, 2014.

[25] J. H. Kim, S. Lee, H. Shin, K.-Y. Jung, H. Choo, and Y. B. Park, "Radiation from a cavity-backed circular aperture array antenna enclosed by an FSS radome," *Appl. Sci.*, vol. 8, no. 12, pp. 2346–2354, Nov. 2018.
[26] D.-C. Son, H. Shin, Y. J. Kim, I. P. Hong, H. J. Chun, K.-Y. Jung, H. Choo, and Y. B. Park, "Design of a hemispherical reconfigurable frequency selective surface using water channels," *IEEE Access*, vol. 6, pp. 61445–61451, 2018.
[27] H. Shin, D. Yoon, D.-Y. Na, and Y. B. Park, "Analysis of transmission loss and boresight error of a curved FSS radome-enclosed antenna," *IEEE Access*, vol. 9, pp. 95843–95852, 2021.
[28] H. Shin, D.-C. Son, S. Lee, J. Lee, S. Choi, H. An, and Y. B. Park, "Radar cross section of a hemisphere FSS radome mounted on a circular cylinder," in *Proc. Int. Symp. Antennas Propag.*, Busan, South Korea, 2018, pp. 171–172.
[29] H. Shin, D. Yoon, and Y. B. Park, "Analysis of radar cross section of a FSS radome mounted on a cylindrical PEC body," presented at the IEEE Int. Symp. Antennas Propag., USNC-URSI Radio Sci. Meeting, Atlanta, GA, USA, Jul. 2019.
[30] H. Shin, D. Yoon, K. Choi, I. Jung, and Y. B. Park, "Analysis of a curved multi-layer radome using a flat model and the ray tracing technique," *J. Electr. Eng. Technol.*, vol. 15, no. 2, pp. 787–794, Mar. 2020.
[31] (2019). *Ansys HFSS*. [Online]. Available: http://www.ansys.com/
[32] (2021). *CST Microwave Studio*. [Online]. Available: https://www.cst.com/
[33] A. Baussard, M. Rochdi, and A. Khenchaf, "PO/MEC-based scattering model for complex objects on a sea surface," *Prog. Electromagn. Res.*, vol. 111, pp. 229–251, 2011.
[34] Y. Bennani, F. Comblet, and A. Khenchaf, "RCS of complex targets: Original representation validated by measurements—Application to ISAR imagery," *IEEE Trans. Geosci. Remote Sens.*, vol. 50, no. 10, pp. 3882–3891, Oct. 2012.
[35] C. A. Balanis, *Advanced Engineering Electromagnetics*, 2nd ed. New York, NY, USA: Wiley, 2012.

HOKEUN SHIN (Member, IEEE) received the B.S. degree in electrical and computer engineering and the integrated M.S. and Ph.D. degree in AI convergence network from Ajou University, Suwon, South Korea, in 2015 and 2021, respectively. He is currently a Senior Engineer at Hanwha Systems, Seongnam, South Korea. His research interests include electromagnetic field analysis, high-frequency techniques, frequency selective surface, radomes, and radar cross section.

DAEYEONG YOON (Student Member, IEEE) received the B.S. degree in electrical and computer engineering from Ajou University, Suwon, South Korea, in 2018, where he is currently pursuing the integrated M.S./Ph.D. degree in AI convergence network. His research interests include frequency selective surface, radomes, and radar cross section.

DONG-YEOP NA (Member, IEEE) received the B.S. and M.S. degrees in electrical and computer engineering from Ajou University, Suwon, South Korea, in 2012 and 2014, respectively, and the Ph.D. degree in electrical and computer engineering from The Ohio State University, Columbus, OH, USA, in 2018. He is currently a Research Scientist at Purdue University. His research interests include computational electromagnetics, kinetic plasma modeling via particle-in-cell algorithm, and quantum electromagnetics.

YONG BAE PARK (Senior Member, IEEE) received the B.S., M.S., and Ph.D. degrees in electrical engineering from the Korea Advanced Institute of Science and Technology, South Korea, in 1998, 2000, and 2003, respectively. From 2003 to 2006, he was with the Korea Telecom Laboratory, Seoul, South Korea. He joined the School of Electrical and Computer Engineering, Ajou University, South Korea, in 2006, where he is currently a Professor. His research interests include electromagnetic field analysis, high-frequency methods, metamaterial antennas, radomes, and stealth technology.